1,6-Hexanedithiol Self-Assembled Monolayers on Au(111) Investigated by Electrochemical, Spectroscopic, and Molecular Mechanics Methods

Deyu Qu, Byung-Cheol Kim, and Chi-Woo J. Lee*

Department of Advanced Materials Chemistry, College of Science and Technology, Korea University, Jochiwon, Choongnam 339-700, Korea

Mikio Ito, Hidenori Noguchi, and Kohei Uosaki*

Physical Chemistry Laboratory, Division of Chemistry, Graduate School of Science, Hokkaido University, Sapporo 060-0810, Japan

Received: September 12, 2009; Revised Manuscript Received: November 12, 2009

1,6-Hexanedithiol (HSC_6SH) self-assembled monolayers (SAMs) on Au(111) were formed in a 1 mM ethanolic solution and were investigated by voltammetry in 0.1 M aqueous KOH solution. HSC_6SH SAMs on Au(111) were further probed by X-ray photoelectron spectroscopy (XPS), scanning tunneling microscopy (STM), sum frequency generation spectroscopy (SFG), and molecular mechanics calculation (MMC). An identical investigation was performed with the self-assembly of hexanethiol (C_6SH) on Au(111) for comparison. Linear sweep voltammograms showed that a full monolayer of thiolate (7.6 ($\pm$0.2) $\times$ 10^{-10} mol^{-2}) chemisorbed on Au(111) with both HSC_6SH and C_6SH, while the peak potential of the electroreduction of the former assembly was more negative than that of the latter. XPS revealed that two different forms of sulfur existed at HSC_6SH SAMs on Au(111), i.e. a thiolate and a thiol. The STM image could not be resolved with HSC_6SH SAMs, while it was atomically well-defined with the C_6SH case. SFG results showed that alkyl chains within the HSC_6SH SAMs were in an all-trans conformation. Thus the experimental results concluded that densely packed and higly oriented HSC_6SH SAMs could be successfully formed on Au(111) with the incubation conditions in the practical solution. MMC presented that HSC_6SH SAMs were more stable than C_6SH ones because of the additional end−end interaction among the thiol groups faced up to the air, albeit both SAMs were tilted by 28° from the surface normal.

Introduction

Self-assembled monolayers (SAMs) of organic thiols on gold have been extensively studied for the past few decades.[1−3] They are good molecular candidates to be used in many application areas as well as highly reproducible model systems for understanding organic interface.[1−3] Among many applications, molecular nanoelectronics is receiving interest as the most attractive field, in which the organic molecules are used as a key electronic component. SAMs with ω-functional groups have been widely used for this purpose because of their unique advantages such as ease of preparation, highly ordered structure, and well-documented properties.[4−27] The functionalities on the top of SAMs mainly control the surface properties of the organic film. Among them, thiol-terminated surfaces, with their high affinity to metals, can serve as templates for the formation of metal film or metal wires at the SAM−ambient interface by preventing the diffusion of metal into SAMs and the formation of a short circuit.[4−7,14−17,22,23,27−29] The most suitable constituent for the formation of a thiol-terminated SAM is dithiol. Dithiol SAMs have been utilized to make nanodevices, for measurements of electricity transport, and for multilayer formation.[4−7,14−17,22,23,25,30−40] So far, most studies have focused on their use either as a linker for metal nanoparticles to study charge transfer or as a spacer for multilayer formation. Compared to the well-studied monothiolate SAMs, not many reports have focused on the growth and structure of dithiol SAMs, and disagreements exist among the literature reported concerning the preparation of dithiol SAMs, the resulting structures, and the quality of dithiol SAMs. 1,6-hexanedithiol (HSC_6SH) on Au(111) has been a case of interest and controversy in the literature[29,30,33−35,41−45] and was examined in this study.

Scoles et al. carefully studied monolayers of HSC_6SH on Au(111) single-crystal substrates by means of several surface science techniques in vacuum, and reported that the molecules lay prone in a striped arrangement with an inter-row spacing of 5 Å from the gas phase and that no evidence of nucleation of other ordered phases was found in different growth protocols, including liquid-phase deposition of 4−16 h in a millimolar ethanolic solution.[41] The results were then explained by the strong molecule/substrate interaction in the striped phases, which was interpreted as a consequence of the strong, but, not site-specific, interaction of both sulfurs with the gold surface. This looping construction will impede the formation of thiol-terminated SAMs and inhibit their application in molecular electronics, as was pointed out in their work.[41] Recently, the same group asserted the importance of the problem again.[42] On the other hand, Bard et al. used HSC_6SH as a linker to construct a copper(I)−dithiol multilayer thin film, which was evidenced by ellipsometric, X-ray photoelectron and fluorescence spectroscopic, and electrochemical techniques.[30] HSC_6SH was also used for the preparation of CdS nanoparticle−dithiol multilayer by one of us[33,34] and Alivisatos.[43] HSC_6SH used to immobilize

* To whom correspondence should be addressed. (C.-W.L.) Phone: +82-41-860-1333; fax: +82-41-867-6823; e-mail: cwlee@korea.ac.kr. (K.U.) Phone: +81-11-706-3128; fax: +81-11-706-3440; e-mail: uosaki@pcl.sci.hokudai.ac.jp.

10.1021/jp908821b
Published on Web 12/16/2009

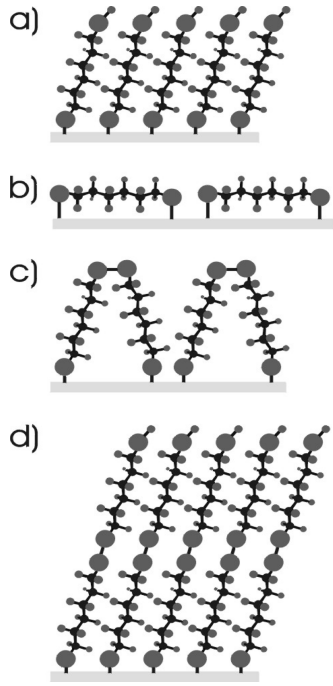

Figure 1. Schematic illustration of various possible configurations of HSC_6SH molecules adsorbed on Au(111) substrate.

a Au nanoparticle on a Au surface was reported recently.[29] A spontaneous robust multilayer formation up to eight layers through disulfide linkage by using this molecule as a spacer was also reported by the Blanchard research group.[35] In that study, HSC_6SH was claimed to adsorb on a gold surface as monothiolate via only one thiol functionality and was shown to have an upright molecular structure for the linking chemistry between layers to take place.[35] With this configuration, one free thiol group of HSC_6SH SAMs is pendent with respect to the Au substrate and serves as the platform for the applications. Yi et al. demonstrated that a monolayer of HSC_6SH SAMs could be monitored to be formed on Au under argon atmosphere within 1 h and remained for hours in 1 mM ethanolic solution by time-resolved surface plasmon resonance measurements, while stepwise multilayers under atmospheric conditions could be formed within the period of several hours.[44] They estimated a tilt angle of 39° on the basis of a comparison between the experimental (6.9 Å) and theoretical (10.9 Å) values. By using a micromechanical cantilever sensor and a molecular simulation study, Hope-Weeks et al. monitored the formation of SAMs of alkanedithiols.[45] They concluded that hexanedithiol adsorbed onto the gold surface via only one thiol group. An upright molecular structure model with formation of an intralayer disulfide bond on the top of HSC_6SH SAM was also proposed.[26,47] The formation of the intralayer disulfide linkage was suggested to take place spontaneously in the presence of trace oxidants and to cause a rearrangement of molecular configuration of HSC_6SH molecules in the SAM.[26,47] Thus, formation of HSC_6SH SAMs on Au appears to be a sensitive function of the experimental variables involved during the preparation, and apparently conflicting results exist in the literature on the formation and structure of and chemistry at HSC_6SH SAMs on Au. However, a well-established protocol with convenient medium would be beneficial for the successful application of this molecular system to relevant fields.[46]

The various possible configurations of HSC_6SH molecules on Au are shown in Figure 1.

In this study, a densely packed, looping structure-free, thiol-terminated HSC_6SH SAM (as shown in Figure 1a) with higher stability than that of the monothiol hexanethiol (C_6SH) SAM was prepared. The kinetic process of HSC_6SH SAM formation was investigated by means of electrochemical measurements, because electrochemistry surveys the quality of the entire SAMs on Au. These thiol-terminated HSC_6SH SAMs were then examined by X-ray photoelectron spectroscopy (XPS), sum frequency generation (SFG), and scanning tunneling microscopy (STM). As a comparison, C_6SH SAMs were also investigated. With the aid of theoretical calculation, the structure of an HSC_6SH SAM on Au was presented. Our goal was to clarify previous contradictions and to provide information on the formation kinetics, structure, quality, and stability of HSC_6SH SAMs on Au(111) substrate. The possibility of the formation of disulfide was also discussed.

Experimental Section

Materials. HSC_6SH (>96%), C_6SH (>95%), and KOH (semiconductor grade) were purchased from Aldrich. Ethanol (reagent grade) and H_2SO_4 (suprapure grade) were obtained from Wako Pure Chemicals. All chemicals were used as received. Water was purified using a Milli-Q purification system (Millipore). Ultrapure Ar gas (99.9995%) was purchased from Air Water.

A Au(111) single crystal was prepared from a gold wire (99.999% pure, Tanaka Precious Metal) by the Clavilier method and was then cut and mechanically polished.[23,48] The real surface area of the Au(111) single-crystal electrode was estimated from the cathodic current corresponding to the reduction of Au oxide to be 0.078 cm^2. STM observations were carried out on an atomically flat (111) facet formed on the surface of a gold single-crystal bead. The gold substrates used for SFG measurements were prepared by vacuum evaporation. Titanium of 10 nm in thickness was evaporated on a slide glass followed by 100-nm-thick gold evaporation at an evaporation rate of 0.01 nm s^{-1} at 200 °C. The gold surface was flame-annealed in a hydrogen flame and cooled under an argon stream before each measurement.

Electrochemical Measurements. Electrochemical measurements were performed in a three-compartment electrochemical cell using an EG&G 283A potentiostat. The electrode potential was referred to a Ag/AgCl electrode, and a Pt wire was used as the counter electrode. The electrolyte solution was deaerated by bubbling Ar gas for at least 30 min before each experiment.

STM. STM measurements were carried out by using a NanoScope E (Digital Instrument) or a PicoSPM (Molecular Imaging). STM images were obtained in constant current mode. STM tips were prepared from Pt−Ir (8:2) wire (Tanaka Precious Metal or California Fine Wire Company) by the mechanical cutting method.

XPS. XP spectra were obtained using a PHI 5800 ESCA System with Al Kα radiation. Base pressure in the analysis chamber was 5×10^{-7} Pa. Wide scans were carried out with 50 eV pass energy, 25 W electron-beam power, and a resolution of 0.8 eV. Narrow-scan spectra of the S 2p and Au 4f regions were taken with 15 eV pass energy, 100 W electron-beam power, and a resolution of 0.1 eV. All the binding energy was calibrated with an Au $4f_{7/2}$ peak at 84.0 eV.

SFG. A detailed description of the SFG system has been described elsewhere.[49] Briefly, The loosely focused visible (10 ps duration, 10 cm^{-1} bandwidth, 4 μJ/pulse energy) and broad-bandwidth IR (100 fs duration, 200 cm^{-1} bandwidth, 2 μJ/pulse energy) beams were overlapped at a sample surface. The incident angle of the visible and IR were about 51 and 73 degrees, respectively. The SF light generated from the sample surface was detected by a spectrograph (Oriel Instruments, MS-257)

and an ICCD multichannel detector (Andor, *i*Star). The SFG spectrum was obtained by dividing the ICCD output of the sample by that of GaAs. In the present experiment, polarization of the SFG, VIS, and IR beams to obtain SFG spectra were p, p, and p, respectively, and SFG spectra were analyzed by using the following equation:[50]

$$I_{SFG} = \left| X_{NR}^{(2)} + \frac{A_0 e^{i\varphi}}{\omega - \omega_0 + i\Gamma_0} \right| \quad (1)$$

where ω is the infrared frequency, $\chi_{NR}^{(2)}$ is the nonresonant contribution to the surface nonlinear susceptibility, and ω_0, A_0, φ, and Γ_0 are the resonant frequency, transition amplitude, phase difference between resonant and nonresonant terms, and homogeneous width, respectively.

SAMs Preparation. C_6SH was self-assembled on a Au(111) surface simply by immersion of Au(111) substrate into an ethanolic solution containing 1 mM C_6SH for 12 h. The HSC_6SH SAMs were prepared by immersing the Au(111) substrate in an ethanol solution of HSC_6SH with a concentration of 1 mM for a certain period of time (varied from 1 min to 10 h). The HSC_6SH solutions were saturated with Ar before the incubation. The process of HSC_6SH SAM formation was kept under Ar atmosphere and in the dark to minimize the oxidative formation of disulfide.

Theoretical Method and Molecular Modeling. Molecular modeling calculations for SAMs and single thiol molecules bound to a gold surface were performed with the HyperChem (Hypercube, Inc.) software program on a PC with an Intel Pentium D 2.66 GHz microprocessor.[51]

The three-dimensional structure for C_6SH and HSC_6SH molecules are drawn by using the "model build" function in the software. A stable structure was obtained through "geometry optimization" using ab initio quantum mechanical calculation to express potential energy as a function of atomic configuration. The basis set used in ab initio calculation was "6-31G*". The results of the calculation included atomic charges for each atom. Those atomic charges were used to calculate the electrostatic term of potential energy in molecular mechanics.

The gold single-crystal structure was obtained from a child program of HyperChem, "crystal builder".[52] The Au(111) surface coordinates were achieved manually by rotating the coordinates of the crystal in a proper direction to find the cross section of Au(111) and eliminating the atoms below and above the (111) plane. The C_6SH and HSC_6SH molecules then deposited on the Au(111) surface with a fixed distance around 5 Å, which represented the SAMs, and are shown in Figure 2. The SAM structure contained 37 C_6SH or HSC_6SH molecules. As shown in Figure 2a, the center molecule was encircled by 6, 12, and 18 molecules as the first, second, and third layers of surrounding molecules, respectively. In this configuration, the center molecule was used as a representative of the molecules in SAM.

Molecular Mechanics+ (MM+) force field, which is an extension of MM2, developed by Allinger and co-workers to represent the potential energy, was used in this study.[53]

The Au, S, C, and H atoms were represented by yellow, red, cyan, and gray spheres, respectively. The SAM is composed of 37 single (di)thiol molecules with a fixed distance of 5 Å between two molecules.

The structures obtained through the performance of "geometry optimization" until the root-mean-square (rms) gradient reached 0.1 (kcal/ Å mol) are not optimum geometry, because the potential energy surfaces are too complex for simple geometry optimization to find the real optimum structure. To find the real optimum structures, a molecular dynamics simulation for 100 ps with holding the coordinates of all Au atoms was performed and followed by a second molecular dynamics simulation for 1 ns, which started from the final structure of the first simulation. The purpose of first simulation was just to find the stable structures of SAM, and the second simulation was used to understand the dynamic structural properties of SAMs. A constant temperature of 300 K was used in the simulation, and the snapshots were collected every 0.1 ps.

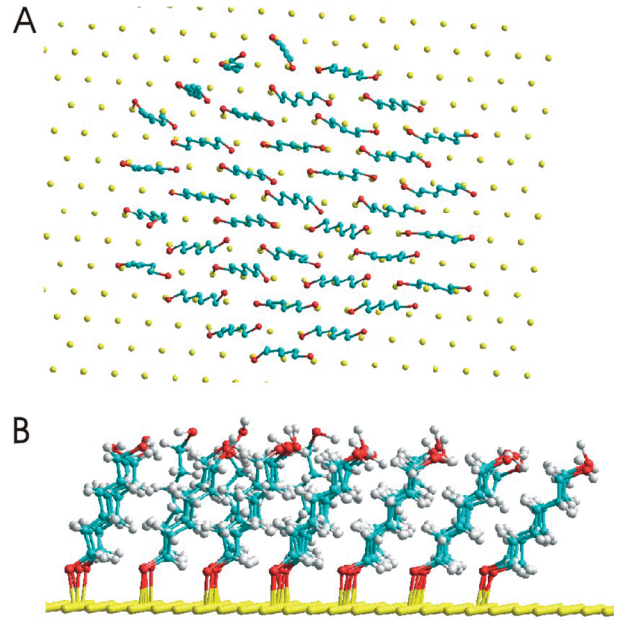

Figure 2. Simulated structure of an HSC_6SH SAM on a Au(111) substrate: (A) top view; (B) side view.

The angles of the C_6SH and HSC_6SH molecules in SAMs with respect to the surface normal of the Au(111) substrate were analyzed. By comparing the calculated angles with the well-known experimental values, the validity of the present calculation was justified.

One of the purposes of the present calculation was to determine the stabilization energy of (di)thiol molecules in SAMs due to their intermolecular interactions. To achieve this, the energy of the center molecule in each SAM was used. One hundred snapshots with the same intervals from the result of 1 ns molecular dynamics for every SAM on Au(111) were collected. The energy of each snapshot was calculated by performing "single-point" calculation.

Results and Discussion

Linear Sweep Voltammogram. Although the previous works extensively relied on surface techniques to probe the formation, structure, and quality of HSC_6SH on a Au electrode,[30,33−35,41,44] an electrochemical method was chosen to investigate them in this study because electrochemistry is an integrative technique, while spectroscopic techniques are inherently local probes. To obtain the information of the kinetic process of HSC_6SH adsorption on a Au substrate, the process of HSC_6SH SAM formation was investigated by means of linear sweep voltammograms (LSVs). The linear sweep reductive desorption measurements were carried out after the Au(111) electrode was incubated in an HSC_6SH solution for various periods of time. The Au(111) single crystal electrode was placed in an ethanol solution containing 1 mM HSC_6SH with a hanging meniscus configuration so that only the Au(111) single crystal surface was exposed to the HSC_6SH solution.

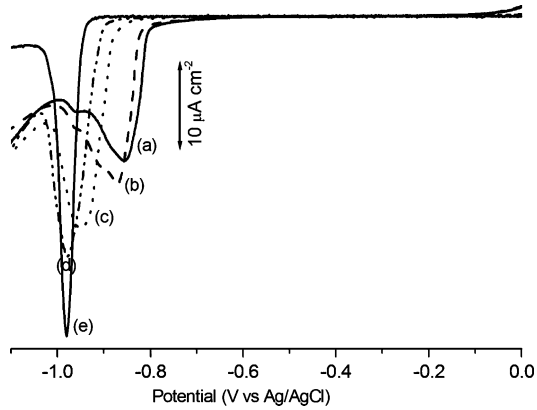

Figure 3. LSVs of HSC_6SH SAM on a Au(111) electrode incubated in a 1 mM HSC_6SH solution for (a) 1 min, (b) 8 min, (c) 30 min, (d) 60 min, and (e) 180 min in 0.1 M KOH solution with a potential scan rate of 20 mV s^{-1}.

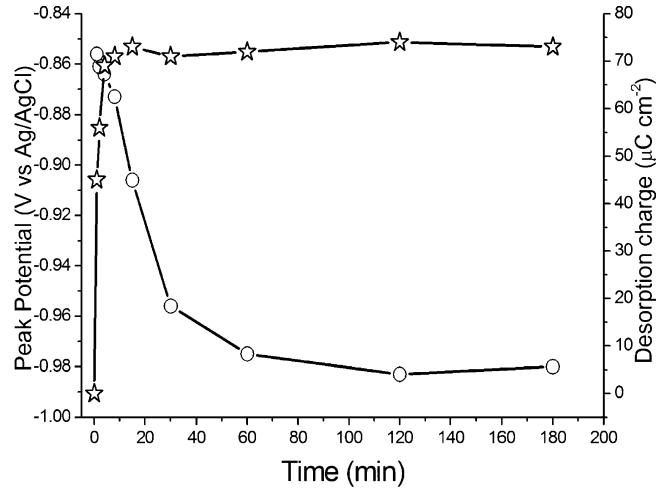

Figure 4. Reductive desorption peak potential (circles) and charge of the cathodic wave (stars) as a function of incubation time.

Figure 3 shows the LSVs obtained in a 0.1 M KOH solution from 0 to −1.1 V at a scan rate of 20 mV s^{-1} after the electrode was incubated in the HSC_6SH solutions for various periods of time. A series of reductive current peaks associated with different formation times was observed. Those peaks were assigned to represent the desorption of hexanedithiolate (HSC_6S) from the Au(111) surface, in which the gold−sulfur bond was broken in this reductive process. Generally, thiol SAMs are known to undergo the reductive desorption when a negative potential is applied to the Au electrode.[54−68] In this process, charge is transferred from Au to the thiols, and most of the desorbed thiolates are diffused away from the Au surface. The electrochemical half reaction is $RS{-}Au + e \rightarrow RS^- + Au$.[55,59−61,63−66] It should be noted that the reductive desorption current peak contains two components. The most important one is the charge transfer between the electrode and the chemisorbed thiols (Faradic process), and the other is a smaller capacitive component linked to the formation of the double layer on the uncoated gold electrode after thiol removal (non-Faradic process).[59−61,63−66] The potential at which the thiolate desorption occurs was found to be strongly dependent on a number of factors, such as chain-length, degree of ordering, various forms of intermolecular interactions within the SAMs, crystallinity of the substrate and so on.[59−61,66,67] Therefore, the area, shape, and position of the reductive desorption peak provide useful information on the adsorption state of SAMs, such as the adsorbed amount, stability, adsorption energy, orientation, and substrate morphology. For example, it was found that the longer the alkyl chain was, the more negative the reductive peak potential was, reflecting that the van der Waals attractive interaction among alkyl chains was a significant contributor to the shift.[55−64,67]

It can be seen in Figure 3 that the peak area increased and that the peak position shifted negatively as the adsorption time was increased. The shape of the reductive desorption peak was also found to change from broad to relatively sharp when the incubation time was increased. Since the area and position of the cathodic peak reflected the amount of adsorption and the order of SAM, respectively,[1,2,54−68] the incubation time dependence of the potential and integrated charge of the reductive desorption peaks is summarized for further analysis in Figure 4. The charges associated with the reductive desorption of HSC_6SH SAMs at different adsorption times were obtained by the integration of charge from LSVs with double-layer charge correction, and only Faradic charge was presented. Figure 4 shows that the reductive charge increased as the incubation time increased and reached 74 $\mu C\ cm^{-2}$ at around 10 min. It is well-known that the reductive desorption of alkanethiolate from Au substrate is a one-electron process,[55] and therefore this Faradic charge (74 $\mu C\ cm^{-2}$) amounts to a thiolate surface concentration of 7.5×10^{-10} mol cm^{-2}. This is in good agreement with the surface concentration calculated from an alkanethiolate SAM in the $(\sqrt{3})\ R\ 30°$ structure formed on a Au(111) surface, which gave a saturated coverage value of 7.6×10^{-10} mol cm^{-2}.[55−68] This result suggests that a full coverage of HSC_6SH on the Au(111) substrate surface was indeed formed and excluded the formation of a looping structure in this dithiol SAM. The observed charge is different from the previous studies, in which a 130 $\mu C\ cm^{-2}$ reductive charge of HSC_6SH SAMs was observed and a partially formed intralayer disufide bond on the top of the dithiol SAMs was proposed.[26,47] This result indicates that the intralayer disulfide bond was not formed in the present case and that the rearrangement of HSC_6SH molecular configuration did not occur here.

The peak position of the reductive desorption was also found to be shifted negatively in Figure 4, reflecting an increase in the stability of the HSC_6SH SAMs with the adsorption time increased. It is interesting to note that the peak position continued to shift negatively even after the saturated coverage had been reached. Although the saturated coverage was reached within 10 min, the negative shift of the cathodic peak continued for more than 1 h. This shows that the order of the HSC_6SH SAMs was still low even when the full coverage had been reached, and that the reorganization and ordering of the SAM continued to achieve a highly ordered SAM as the incubation time increased. This observation agrees with the biphasic adsorption kinetics found in the monothiolate SAM formation.[1,2,69−74] This two-step formation process includes a very fast step, which takes a few minutes, followed by a slow step, which lasts for hours. It is thought that the first step is governed by the surface−headgroup reaction, and the slow step is related to a surface crystallization process, where alkyl chains get out of the disordered state and form a two-dimensional crystal state, and therefore the peak position is decided by the chain disorder, the different components of intermolecular interaction, and so on.[1,2,54] It is well-known that, in the case of alkanethiol SAMs on Au(111), the negative shift in the reductive peak potential arises from the decrease in the fractional drop of the applied voltage across the sulfur headgroup as the length of the alkyl chain increases and from the cohesive interactions between polymethylene chains.[55,57,67] We think the same things operate

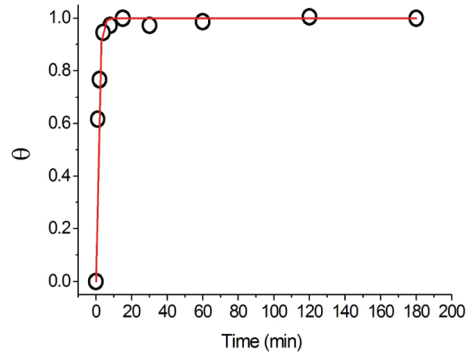

Figure 5. Plot of surface coverage (θ) versus time during the adsorption from 1 mM hexanedithiol. The solid line corresponds to the fit of the Langmuir model according to eq 4.

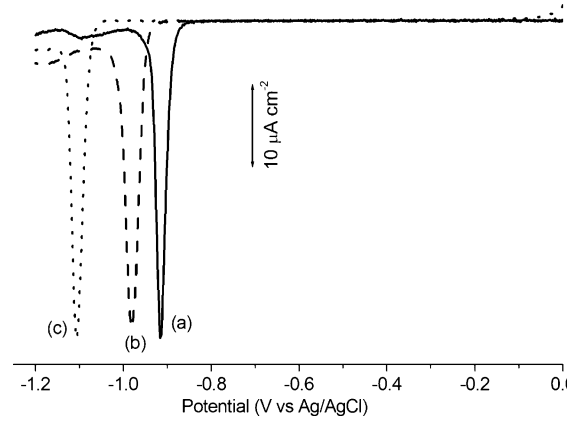

Figure 6. LSVs of (a) C_6SH SAM (solid line), (b) HSC_6SH SAM (dashed line), and (c) HSC_6SH bi/multilayer (dotted line) on a Au(111) electrode in 0.1 M KOH solution with a potential scan rate of 20 mV s^{-1}.

in the case of the dithiol examined in the present work. It is interesting to note that a shoulder peak around −0.95 V along with a broad peak at the peak potentials of −0.85 and −0.86 V appeared in the LSV with incubation times of 1 and 8 min, respectively. The broad peak at the positive potential was the major one, and it was suggested to correspond to a SAM with a disordered state existing in the early stage of SAM formation. On the other hand, the shoulder peak was a minor one, and its position was similar to that in the LSV at 30 min incubation, suggesting that a relatively ordered SAM structure was partially formed, even with short formation times.

To further assess the HSC_6SH adsorption behavior, the kinetic process of the HSC_6SH self-assembly formation on Au(111) surface was analyzed. On the basis of the electrochemical measurements (Figure 3 and 4), the coverage θ can be expressed as a function of the reaction time. The surface coverage θ can be obtained as

$$\theta = Q_t/Q_{Full} \tag{2}$$

where Q_t is the integrated charge of the reductive desorption peak at the incubation time t, and Q_{Full} is the charge of a full monolayer. A plot of surface coverage vs time during the adsorption of HSC_6SH from the 1 mM solution is shown in Figure 5. The well-known Langmuir monolayer adsorption model was employed to fit this adsorption curve.[74−76] If the adsorption process follows this model, the rate of the surface adsorption is governed by the Langmuir isotherm, which is given by

$$d\theta/dt = k_a(1 - \theta)C - k_d\theta \tag{3}$$

where k_a and k_d are the intrinsic rate constants of adsorption and desorption, respectively, and C is the concentration of adsorbate. Since the desorption process is negligible or $k_d \ll k_a$,[74,75] with the substitution of $k_{obs} = k_aC + k_d$, eq 3 gives rise to

$$\theta = 1 - \exp(-k_{obs}t) \tag{4}$$

The observed results were then fitted to eq 4. The solid line in Figure 5 represents the best fit to the experimental data with the adsorption rate constants (k_{obs}) of 0.78 min^{-1}, which is 1 order of magnitude higher than that of the charged monothiol ($HSC_{10}COO^-$) adsorbed on Au.[75] The excellent fit of the data to the Langmuir model should not be thought to imply that all the assumptions in the model are valid in the current situation, especially the intermolecular interaction assumption. It may be thought that identical intermolecular interactions exist with the SAM.

The LSV of HSC_6SH SAMs on a Au(111) substrate formed from 3 h incubation was recorded in a 0.1 M KOH solution at a potential scan rate of 20 mV s^{-1} and is shown in Figure 6 as a dashed line (line b). In this circumstance, the hexanedithiol SAM was thought to reach its saturated coverage with highly ordered configuration. The LSV of the C_6SH SAM was also recorded and is shown in Figure 6 as a solid line (line a). The sharp cathodic peak of −0.92 V corresponding to the reductive desorption of the monothiolate, C_6S, agrees with the one reported in the previous studies.[55,58] Meanwhile, the peak potential of the reductive desorption of the dithiol (HSC_6SH) SAM was found at −0.98 V, around 60 mV negatively shifted from that of the monothiol SAM. This negative shift in the peak position reflects an increase in the stability of the HSC_6SH SAM, i.e., attractive interaction among the adsorbed molecules, compared to that of the C_6SH SAM. Several interactions are known to be involved in the organothiol SAMs on Au substrate, including S−Au interaction, chain−chain interaction, and end group−end group and end group−environment interactions.[1,2,54,59,67,77] The overall balance of those interactions governed the structure and stability of the SAMs, and can be characterized from reductive desorption potential.[59,67,77] Since all those interactions give additive contribution to the reductive desorption peak, and it is reasonable to assume that the energies of S−Au interaction and chain−chain interaction are invariant for both HSC_6SH and C_6SH SAMs, the additional intermolecular end group interaction on HSC_6SH SAMs is likely to be the main reason for the observed change in the reductive desorption potential. Therefore, this negative shift in the reduction peak potential of HSC_6SH SAMs from that of C_6SH ones could be attributed to the S−S interactions on HSC_6SH SAMs which provided their higher stability compared to that of C_6SH SAMs.

All the above experiments were performed under deaerated atmosphere and in the dark. To see the effect of air during the SAM preparation step, HSC_6SH SAMs were prepared under the air atmosphere. LSV c in Figure 6 (dotted line) shows the reductive desorption of the hexanedithiol layer on Au(111) formed from 10 h incubation in a 1 mM HSC_6SH solution, which was exposed to the air. The peak potential and the reductive charge were −1.11 V and 75 $\mu C\ cm^{-2}$, respectively. The observed peak potential was more negative than that of the reductive desorption of HSC_6SH SAMs prepared under inert atmosphere. Since the observed charge was still around 75 $\mu C\ cm^{-2}$, the negative shift in the peak potential was not due to the formation of the intralayer disulfide bond on the top of SAM,

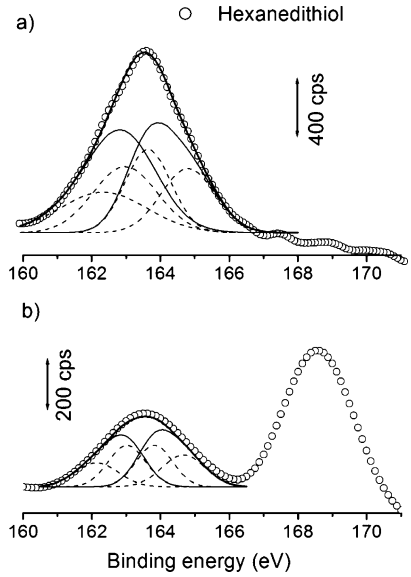

Figure 7. XP spectra of the S 2p region of HSC_6SH SAMs on a Au(111) substrate recorded (a) directly after SAM formation and (b) after 3 weeks of contact with air/light. Dashed lines show two sets of doublets (i.e., Au−SR and RSH). Thin and thick lines represent the sum of each doublet and their total, respectively.

as was suggested to be formed in the previous studies.[26,47] Instead a hexanedithiol bilayer and/or even multilayer structure, via an interlayer disulfide linkage between the thiols of the hexanedithiols in the neighbor layers, was proposed to be formed under the experimental conditions, because this peak potential was more negative than that of the reductive desorption of dodecanethiol ($C_{12}SH$) SAMs on Au(111) surface, which was reported to be −1.07 V.[55] The peak potential change was due to the increase of chain-length interaction in this case. It was still surprising to see that almost the same reductive desorption charge was found in both hexanedithiol multilayer and monolayer structure. The dissociation of disulfide bond did not take place simultaneously with the breaking of the S−Au bond. The reason may be that the bond energy of the disulfide is higher than that of the Au−S bond[78] and that the formed disulfide linkage here is buried in the middle of the bi/multilayer SAM structure. So breaking this interlayer disulfide bond will be more difficult than breaking the intralayer disulfide bond that existed on the top of the SAM in the previous studies.[26,47] After dissociation of the Au−S bond, the desorbed thiolates were thought to leave the electrode surface, and the interlayer disulfide linkages were considered not available for the charge transfer reaction with the electrode.

XPS and STM. The XP spectrum in the S 2p region of HSC_6SH SAMs coated on a Au(111) is presented in Figure 7a. The position of this S 2p peak was found at 163.6 eV, which can be best fit with the two sets of S 2p doublets. Each doublet corresponds to S $2p_{3/2}$ and S $2p_{1/2}$. In one set of doublets, the S $2p_{3/2}$ and S $2p_{1/2}$ peaks were 162.1 and 163.0 eV, respectively, which were in good agreement with the reported $2p_{3/2}$ chemical shift of a thiolate in alkanethiol SAMs on gold (RS−Au).[79] The other set of doublets, the S $2p_{3/2}$ and S $2p_{1/2}$ peaks, were found to be 163.6 and 164.8 eV, which agreed with that of a thiol in a polycrystalline sample (RSH).[79] This indicated that two types of sulfur species, i.e., Au−SR and RSH, coexisted in HSC_6SH SAMs and suggested that HSC_6SH molecules were attached to gold at one end via a S−Au bond with another thiol group remaining unreacted and faced to the SAM−ambient interface.

The XP spectrum of the HSC_6SH SAM on Au(111) presented in Figure 7b was recorded after 3 weeks of contact with air and light in ambient laboratory conditions. Other than organic thiol and thiolate, a sulfur peak with a binding energy of 169 eV was observed. This S 2p peak was thought to be representative of a sulfonate or sulfonic acid moiety, originating from the oxidation of the thiolate or thiols.[43,80] Note that the thiol/thiolate signal intensity ratio in Figure 7b remained almost the same as that in Figure 7a. This phenomenon indicated that the ratio of Au−S bond and free thiol group was unaffected by the oxidation, suggesting that the oxidation reaction proceeded not only at the −SH group on the top of dithiol SAMs but also at the Au−S bond of the SAM/Au interface. It has been shown in a previous study that a sulfonate peak along with a Au−S peak was observed in the XP spectra when a monothiolate SAM on Au was exposed to O_2/light.[80] Since both thiol (−SH) and thiolate (Au−S) were all oxidized during the exposure experiment to the air and light, the intensity ratio of these two did not change before and after the sample was exposed to air/light.

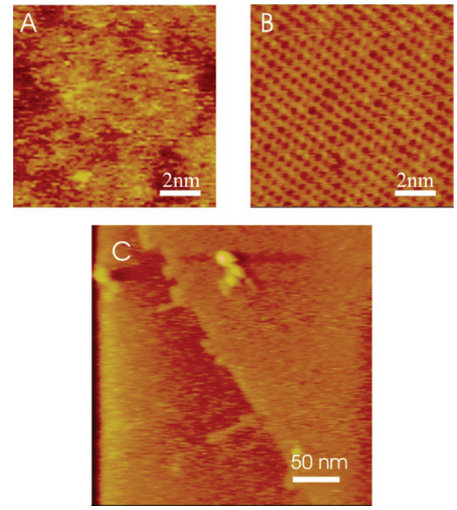

Figure 8. STM images (U_t = 100 mV, I_t = 50 pA) of (A,C) HSC_6SH and (B) C_6SH SAM on a Au(111) substrate.

STM images of HSC_6SH SAMs and C_6SH SAMs on Au(111) are shown in Figure 8A and 8B, respectively. Note that no ordered region can be observed for HSC_6SH SAMs (Figure 8A), and therefore there is no molecular resolution image is present for this dithiol SAM. In the meantime, the molecular resolution image for C_6SH SAMs was obtained (Figure 8B). The lack of ordered image of HSC_6SH SAMs will be temporally attributed to the significant interaction between the Pt tip and the thiol-terminated surface. This is the evidence suggesting that the looplike structure was not present with the HSC_6SH SAMs prepared in this study. Otherwise, the stripe-pattern, which represented the dithiol molecule lying flat on the Au(111) substrate, will be observed.[42] Figure 8C shows the STM image of HSC_6SH SAMs with large scan size (300 nm × 300 nm). A relatively homogeneous image with a single monatomic height step, which separated different terraces on Au(111) surface, was observed. This indicates the formation of HSC_6SH SAMs on Au with an ordered structure.

SFG. SFG spectroscopy has demonstrated to be a powerful tool for the study of structure information of a molecular layer on a solid surface.[49,81−86] It can determine not only orientation and conformational orders, but also the lateral order and symmetry of molecular layers at surfaces. Unlike Fourier transfrom infrared (FT-IR) spectroscopy, a reference spectrum is not required in the SFG measurement because of its high interface sensitivity. Figure 9 shows the SFG spectra of the three samples prepared in this study, namely, (a) HSC_6SH SAMs on

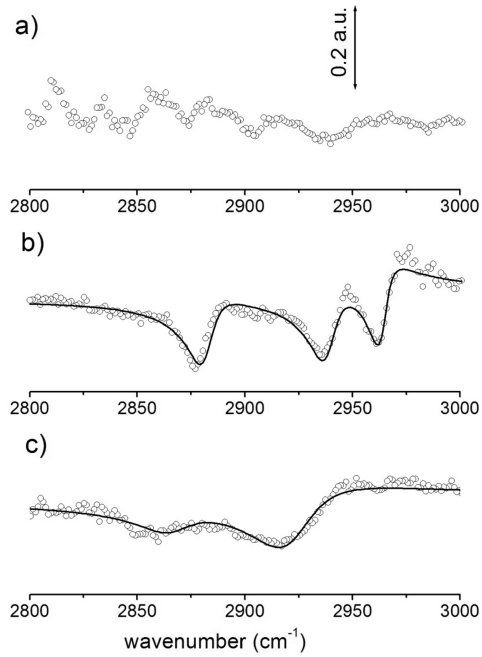

Figure 9. SFG spectra of (a) HSC_6SH SAMs on a Au(111) surface, (b) $C_{10}SH$ SAMs on a Au(111) surface, and (c) metallic Au electrodeposition on an HSC_6SH SAM/Au(111) surface.

a Au(111) surface, (b) $C_{10}SH$ SAMs on a Au(111) surface, and (c) metallic Au electrodeposited on an HSC_6SH SAM/Au(111) surface. The solid lines were the least-squares fitting results obtained using eq 1. Different from the SFG spectrum of monothiol SAMs on a Au(111) surface (Figure 9b), where three peaks were observed at 2880 ($\upsilon_s CH_3$), 2939 ($\upsilon_{s,FR} CH_3$), and 2965 ($\upsilon_{a,ip} CH_3$) cm^{-1}, the spectrum of HSC_6SH SAMs on a Au(111) surface (Figure 9a) shows no peaks. It is well-known that the methylene vibrational modes do not appear in the SFG spectra, if the alkyl chain has all-trans conformation.[85,86] Since there is no methyl group in HSC_6SH molecule, the SFG spectrum of HSC_6SH SAMs (Figure 9a) indicates that the methylene groups in HSC_6SH SAMs were in an all-trans conformation. To further prove that this negative evidence, in which there is no peak observed in the SFG spectrum of hexanedithiol SAMs, is valid in this study, a SFG spectrum was taken after a Au was electrodeposited on the top of this dithiol SAM and is shown in Figure 9c. Two peaks at 2855 and 2914 cm^{-1} in Figure 9c can be assigned to CH_2 symmetric and asymmetric vibration, respectively. This clearly suggests that, once metallic Au deposited on the top of HSC_6SH SAMs, the structure of the alkyl chain was changed, and it was no longer in an all-trans conformation. This observation also supports that the SFG signal in Figure 9a is indeed from the HSC_6SH SAMs. All-trans conformation of the alkyl chain in HSC_6SH SAMs provided another strong evidence that the hexanedithiol SAMs on the Au(111) surface did not form a loop structure, e.g., both of its thiol groups bonded on Au(111) surface (Figure 1b), and supports that the formed hexanedithiol SAM was densly packed and highly oriented. It also can rule out the formation of an intralayer disulfide bond. It is well-known that the distance among thiolates on Au(111) is around 0.5 nm, and that among disulfide is about 0.22 nm.[1,2,87] To form an intralayer disulfide bond, a rearrangement of dithiol molecules in the SAMs is needed as shown in Figure 1c. This change in molecular structure in the SAMs will increase the energy, and break the all-trans configuration of alkyl chain.[47] Since the alkyl chains within the HSC_6SH SAMs were found to be in all-trans

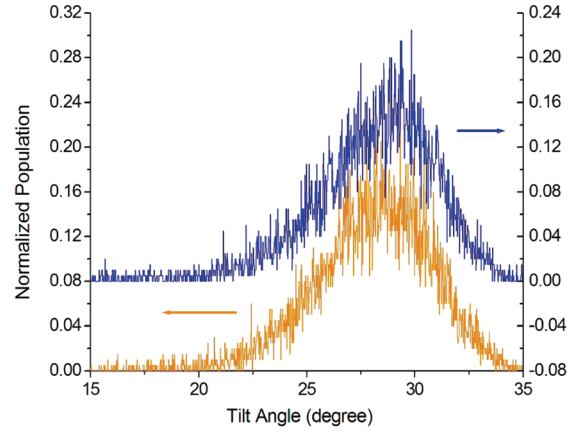

Figure 10. Plot of a normalized population of simulated HSC_6SH (orange) and C_6SH (blue) molecules in each SAM as a function of tilt angles.

configuration by SFG, the formation of an intralayer disulfide bond can be excluded.

Theoretical Calculation. Molecular dynamics calculation for HSC_6SH and C_6SH SAMs were performed for 100 ps followed by a second 1 ns simulation at 300 K. The angles of the HSC_6SH or C_6SH molecules in each SAM with their optimized structure, with respect to the surface normal of the Au(111) substrate, were collected for the second molecular dynamics simulation and plotted as a probability density function or population, as shown in Figure 10. It clearly shows that the tilt angles of both molecules in the SAMs are almost identical and are all around 30°. This is in good agreement with the well-known fact that the title angle for the SAMs of alkylthiol is 30°.[1,2,88] Since the optimized structure of HSC_6SH SAMs is similar to that of corresponding monothiol ones, the alkyl chain of an HSC_6SH molecule in SAMs should have an all-trans conformation, which is consistent with the results of SFG in this study.

The potential energies of SAMs for HSC_6SH and C_6SH were obtained by calculating the potential energy of the center molecule in the SAMs. By doing this, the energy of a center molecule affected by outer molecules can be obtained, and the center molecule here is representative of the entire SAM. The potential energies of HSC_6SH and C_6SH SAMs were found to be 12.9 and 14.7 kcal mol^{-1}, respectively, and clearly indicate that the HSC_6SH SAMs are more stable than C_6SH SAM. This result is compatible with the electrochemical measurements (*vide supra*) very well.

Conclusions

Densely packed and highly ordered HSC_6SH SAMs with an upright molecular structure, in which the dithiol molecules were found to be bound to the substrate via the thiolate link from one of the thiol groups, and the second one was free at the SAM−ambient interface, were formed on a Au(111) substrate from the convenient laboratory conditions. The self-assembly adsorption process of HSC_6SH was studied, and a two-step process—a fast step followed by a slower one—was observed. The fit of a Langmuir adsorption model to the surface coverage versus time yielded an adsorption rate constant of 0.78 min^{-1}. A high stability of hexanedithiol SAMs compared to its corresponding monothiol, C_6SH SAMs, was evidenced by the observation of a negative shift in reductive peak potential from monothiol SAMs to dithiol SAMs. Within hexanedithiol SAMs, two types of sulfur species, i.e., thiolate-type sulfur (Au−SR) and tailgroup thiol sulfur (RSH), were identified by XPS

measurements indicating the stand-up dithiol configuration in the SAMs. The lack of ordered domains for the dithiol SAMs in the STM measurement is consistent with the thiol-terminated surface resulting from the upright dithiol SAM structure, which has a strong interaction with Pt tips. The results of SFG spectra and electrochemical measurements exhibited that a full layer of dithiol SAMs with their alkyl chains in an all-trans configuration was formed on Au(111) surface. The theoretical calculation provided that both C_6SH and hexanedithiol SAMs have a similar structure. The calculated potential energies of C_6SH and hexanedithiol SAMs shows the same trend as observed by experimental means.

Acknowledgment. This work was financially supported by Korea University, 2nd BK21 Materials Chemistry Program, Korea, and partially supported by a Grant-in-Aid for Scientific Research (KAKENHI) in the Priority Area of "Molecular Nano Dynamics" (No. 16072202) from the Ministry of Education, Culture, Sports, Science and Technology, Japan.

References and Notes

(1) Ulman, A. *Chem. Rev.* **1996**, *96*, 1533.
(2) Ulman, A. *An Introduction to Ultra-thin Organic Films from Langmuir−Blodgett to Self-Assembly*; Academic Press: San Diego, CA, 1991.
(3) Love, J. C.; Estroff, L. A.; Kriebel, J. K.; Nuzzo, R. G.; Whitesides, G. M. *Chem. Rev.* **2005**, *105*, 1103.
(4) Boer, B.; Frank, M. M.; Chabal, Y. J.; Jiang, W.; Garfunkel, E.; Bao, Z. *Langmuir* **2004**, *20*, 1539.
(5) Ohgi, T.; Sheng, H.-Y.; Nejoh, H. *Appl. Surf. Sci.* **1998**, *130−132*, 919.
(6) Ohgi, T.; Sheng, H.-Y.; Dong, Z. -C.; Nejoh, H.; Fujita, D. *Appl. Phys. Lett.* **2001**, *79*, 2453.
(7) Andres, R. P.; Bein, T.; Dorogi, M.; Feng, S.; Henderson, J. I.; Kubiak, C. P.; Mahoney, W.; Osifchin, R. G.; Reifenberger, R. *Science* **1996**, *272*, 1323.
(8) Ohgi, T.; Sheng, H.-Y.; Dong, Z. -C.; Nejoh, H. *Surf. Sci.* **1999**, *442*, 277.
(9) Esplandiu, M. J.; Noeske, P. -L. M. *Appl. Surf. Sci.* **2002**, *199*, 166.
(10) Tarlov, M. J. *Langmuir* **1992**, *8*, 80.
(11) Ohgi, T.; Fujita, D.; Deng, W.; Dong, Z.-C.; Nejoh, H. *Surf. Sci.* **2001**, *493*, 453.
(12) Speets, E. A.; Ravoo, B. J.; Roesthuis, F. J. G.; Vroegindeweij, F.; Blank, D. H. A.; Reinhoudt, D. N. *Nano Lett.* **2004**, *4*, 841.
(13) Speets, E. A.; Dordi, B.; Ravoo, B. J.; Oncel, N.; Hallback, A.-S.; Zandvliet, H. J. W.; Poelsema, B.; Rijnders, G.; Blank, D. H. A.; Reinhoudt, D. N. *Small* **2005**, *1*, 395.
(14) Cui, X. D.; Primak, A.; Zarate, X.; Tomfohr, J.; Sankey, O. F.; Moore, A. L.; Moore, T. A.; Gust, D.; Harris, G.; Lindsay, S. M. *Science* **2001**, *294*, 571.
(15) Xiao, Y.; Patolsky, F.; Katz, E.; Hainfeld, J. F.; Willner, I. *Science* **2003**, *299*, 1877.
(16) Ramachandran, G. K.; Hopson, T. J.; Rawlett, A. M.; Nagahara, L. A.; Primak, A.; Lindsay, S. M. *Science* **2003**, *300*, 1413.
(17) Zheng, J.; Zhou, Y.; Li, X.; Ji, Y.; Lu, T.; Gu, R. *Langmuir* **2003**, *19*, 632.
(18) Baunach, T.; Ivanova, V.; Kolb, D. M.; Boyen, H.-G.; Ziemann, P.; Buttner, M.; Oelhafen, P. *Adv. Mater.* **2004**, *16*, 2024.
(19) Ivanova, V.; Baunach, T.; Kolb, D. M. *Electrochim. Acta* **2005**, *50*, 4283.
(20) Manolova, M.; Ivanova, V.; Kolb, D. M.; Boyen, H.-G.; Ziemann, P.; Buttner, M.; Romanyuk, A.; Oelhafen, P. *Surf. Sci.* **2005**, *590*, 146.
(21) Manolova, M.; Kayser, M.; Kolb, D. M.; Boyen, H.-G.; Ziemann, P.; Mayerc, D.; Wirth, A. *Electrochim. Acta* **2007**, *52*, 2740.
(22) Qu, D.; Uosaki, K. *Chem. Lett.* **2006**, *35*, 258.
(23) Qu, D.; Uosaki, K. *J. Phys. Chem. B* **2006**, *110*, 17570.
(24) Riskin, M.; Basnar, B.; Chegel, V. I.; Katz, E.; Willner, I.; Shi, F.; Zhang, X. *J. Am. Chem. Soc.* **2006**, *128*, 1253.
(25) Akkerman, H. B.; Naber, R. C. G.; Jongbloed, B.; van Hal, P. A.; Blom, P. W. M.; de Leeuw, D. M.; de Boer, B. *Proc. Natl. Acad. Sci.* **2007**, *104*, 11161.
(26) Esplandiu, M. J.; Hagenstrom, H.; Kolb, D. M. *Langmuir* **2001**, *17*, 828.
(27) Akkerman, H. B.; Kronemeijer, A. J.; van Hal, P. A.; de Leeuw, D. M.; Blom, P. W. M.; de Boer, B. *Small* **2008**, *4*, 100.
(28) Rajalingam, K.; Strunskus, T.; Terfort, A.; Fischer, R. A.; Woll, C. *Langmuir* **2008**, *24*, 7986.
(29) Sivanesan, A.; Kannan, P.; Abraham John, S. *Electrochim. Acta* **2007**, *52*, 8118.
(30) Burst, M.; Blass, P. M.; Bard, A. J. *Langmuir* **1997**, *13*, 5602.
(31) Deng, W.; Yang, L.; Fujita, D.; Nejoh, H.; Bai, C. *Appl. Phys. A: Mater. Sci. Process.* **2000**, *71*, 639.
(32) Venkataramanan, M.; Murty, K. V. G. K.; Pradeep, T.; Deepali, W.; Vijayamohanan, K. *Langmuir* **2000**, *16*, 7673.
(33) Nakanishi, T.; Ohtani, B.; Shimazu, K.; Uosaki, K. *Chem. Phys. Lett.* **1997**, *278*, 233.
(34) Nakanishi, T.; Ohtani, B.; Uosaki, K. *J. Phys. Chem. B* **1998**, *102*, 1571.
(35) Kohli, P.; Taylor, K. K.; Harris, J. J.; Blanchard, G. J. *J. Am. Chem. Soc.* **1998**, *120*, 11962.
(36) Rifai, S.; Laferriere, M.; Qu, D.; Wayner, D. D. M.; Wilde, C. P.; Morin, M. *J. Electroanal. Chem.* **2002**, *531*, 111.
(37) Rifai, S.; Morin, M. *J. Electroanal. Chem.* **2003**, *550−551*, 277.
(38) Rifai, S.; Lopinski, G. P.; Ward, T.; Wayner, D. D. M.; Morin, M. *Langmuir* **2003**, *19*, 8916.
(39) Haiss, W.; Martin, S.; Leary, E.; van Zalinge, H.; Higgins, S. J.; Bouffier, L.; Nichols, R. J. *J. Phys. Chem. C* **2009**, *113*, 5823.
(40) Wold, D. J.; Frisbie, C. D. *J. Am. Chem. Soc.* **2001**, *123*, 5549.
(41) Leung, T. Y. B.; Gerstenberg, M. C.; Lavrich, D. J.; Scoles, G.; Schreiber, F.; Poirier, G. E. *Langmuir* **2000**, *16*, 549.
(42) Liang, J.; Rosa, L. G.; Scoles, G. *J. Phys. Chem. C* **2007**, *111*, 17275.
(43) Colvin, V. L.; Goldstein, A. N.; Alivisatos, A. P. *J. Am. Chem. Soc.* **1992**, *114*, 5221.
(44) Chah, S.; Fendler, J. H.; Yi, J. *Chem. Commun.* **2002**, *24*, 2094.
(45) Kohale, S.; Molina, S. M.; Weeks, B. L.; Khare, R.; Hope-Weeks, L. J. *Langmuir* **2007**, *23*, 1258.
(46) Li, C.; Pobelov, I.; Wandlowski, T.; Bagrets, A.; Arnold, A.; Evers, F. *J. Am. Chem. Soc.* **2008**, *130*, 318.
(47) Carot, M. L.; Esplandiu, M. J.; Cometto, F. P.; Patrito, E. M.; Macagno, V. A. *J. Electroanal. Chem.* **2005**, *579*, 13.
(48) Clavilier, J.; Faure, R.; Guinet, G.; Durand, R. *J. Electroanal. Chem.* **1980**, *107*, 205.
(49) Noguchi, H.; Ito, M.; Uosaki, K. *Chem. Lett.* **2005**, *34*, 950.
(50) Shen, Y. R. *Nature* **1989**, *337*, 519.
(51) *HyperChem*, release 7.5 for Windows; Hypercube, Inc.: Gainesville, FL.
(52) *HyperChem Manual*; Hypercube, Inc.: Gainesville, FL, 2002.
(53) Allinger, N. L. *J. Am. Chem. Soc.* **1977**, *99*, 8127.
(54) Finklea, H. O. In *Electroanalytical Chemistry*; Bard, A. J., Rubinstein, I., Eds.; Marcel Dekker: New York, 1990; Vol. 19, p 109.
(55) Widrig, C. A.; Chung, C.; Porter, M. D. *J. Electroanal. Chem.* **1991**, *310*, 335.
(56) Walczak, M. M.; Popenoe, D. D.; Deinhammer, R. S.; Lamp, B. D.; Chung, C.; Porter, M. D. *Langmuir* **1991**, *7*, 2687.
(57) Walczak, M. M.; Alves, C. A.; Lamp, B. D.; Porter, M. D. *J. Electroanal. Chem.* **1995**, *396*, 103.
(58) Zhong, C.-J.; Porter, M. D. *J. Electroanal. Chem.* **1997**, *425*, 147.
(59) Kawaguchi, T.; Yasuda, H.; Shimazu, K.; Porter, M. D. *Langmuir* **2000**, *16*, 9830.
(60) Yang, D.-F.; Wilde, C. P.; Morin, M. *Langmuir* **1996**, *12*, 6570.
(61) Yang, D.-F.; Wilde, C. P.; Morin, M. *Langmuir* **1997**, *13*, 243.
(62) Yang, D.-F.; Morin, M. *J. Electroanal. Chem.* **1998**, *441*, 173.
(63) Qu, D.; Morin, M. *J. Electroanal. Chem.* **2001**, *517*, 45.
(64) Qu, D.; Kim, B.-C.; Lee, C.-W.; Uosaki, K. *Bull. Korean Chem. Soc.* **2009**, *30*, 2549.
(65) Sumi, T.; Wano, H.; Uosaki, K. *J. Electroanal. Chem.* **2003**, *550−551*, 321.
(66) Sumi, T.; Uosaki, K. *J. Phys. Chem. B* **2004**, *108*, 6422.
(67) Imabayashi, S.; Iida, M.; Hobara, D.; Feng, Z. Q.; Niki, K.; Kakiuchi, T. *J. Electroanal. Chem.* **1997**, *428*, 33.
(68) Schneider, T. W.; Buttry, D. A. *J. Am. Chem. Soc.* **1993**, *115*, 12391.
(69) Bensebaa, F.; Voicu, R.; Huron, L.; Ellis, T. H.; Kruus, E. *Langmuir* **1997**, *13*, 5335.
(70) Shimazu, K.; Yagi, I.; Sato, Y.; Uosaki, K. *Langmuir* **1992**, *8*, 1385.
(71) Yamada, R.; Uosaki, K. *Langmuir* **1997**, *13*, 5218.
(72) Yamada, R.; Uosaki, K. *Langmuir* **1998**, *14*, 855.
(73) Dannenberger, O.; Buck, M.; Grunze, M. *J. Phys. Chem. B* **1999**, *103*, 2202.
(74) Karpovich, D. S.; Blanchard, G. J. *Langmuir* **1994**, *10*, 3315.
(75) Hu, K.; Bard, A. J. *Langmuir* **1998**, *14*, 4790.
(76) Degenhart, G. H.; Dordi, B.; Schonherr, H.; Vancso, G. J. *Langmuir* **2004**, *20*, 6126.

(77) Schreiber, F. *Prog. Surf. Sci.* **2000**, *65*, 151.
(78) Borsari, M.; Cannio, M.; Gavioli, G. *Electroanalysis* **2003**, *15*, 1192.
(79) Laibinis, P. E.; Whitesides, G. M.; Allara, D. L.; Tao, Y.-T.; Parikh, A. N.; Nuzzo, R. G. *J. Am. Chem. Soc.* **1991**, *113*, 7152.
(80) Rieley, H.; Price, N. J.; Smith, T. L.; Yang, S. *J. Chem. Soc., Faraday Trans.* **1996**, *92*, 3629.
(81) Ishibashi, T.; Ara, M.; Tada, H.; Onishi, H. *Chem. Phys. Lett.* **2003**, *367*, 376.
(82) Ye, S.; Noda, H.; Morita, S.; Uosaki, K.; Osawa, M. *Langmuir* **2003**, *19*, 2238.
(83) Nishi, N.; Hobara, D.; Yamamoto, M.; Kakiuchi, T. *J. Chem. Phys.* **2003**, *118*, 1904.
(84) Lis, D.; Peremans, A.; Sartenaer, Y.; Caudano, Y.; Mani, A. A.; Dreesen, L.; Thiry, P. A.; Gethmuller, J.; Champagne, B.; Cechet, F. *J. Phys. Chem. C* **2009**, *113*, 9857.
(85) Himmelhaus, M.; Eisert, F.; Buck, M.; Grunze, M. *J. Phys. Chem. B* **2000**, *104*, 576.
(86) Nihonyanagi, S.; Miyamoto, D.; Idojiri, S.; Uosaki, K. *J. Am. Chem. Soc.* **2004**, *126*, 7034.
(87) Breitzer, J. G.; Smirnov, A. I.; Szczepura, L. F.; Wilson, S. R.; Rauchfuss, T. B. *Inorg. Chem.* **2001**, *40*, 1421.
(88) Gonzalez-Lakunza, N.; Lorente, N.; Arnau, A. *J. Phys. Chem. C* **2007**, *111*, 12383.

JP908821B